Journal of Computational Applied Mechanics 2026, 57(4): 663-682

DOI: 10.22059/jcamech.2026.420335.1921

RESEARCH PAPER

Modeling and Analysis of a High-Frequency RF MEMS Double-Clamped Beam Resonator for HF Mechanical Filters

K. Kurmendra*

Department of Electronics and Communication Engineering, North Eastern Regional Institute of Science and Technology, Nirjuli-791109, Arunachal Pradesh, India

Abstract

This paper presents a High Frequency RF MEMS double-clamped beam resonator model. It focuses on yielding a resonant frequency in the HF range. Since the resonant frequency of a micromechanical resonator highly depends on its geometry, hence it is considered to be the most important consideration while designing a micromechanical resonator. Therefore, this work presents a close study of geometric dependencies of resonant frequency of a micro-electro- mechanical resonator. A double-clamped beam structure has been used as base resonator which is suspended above the substrate and the conductive strip underlying just below the center of the resonator served as capacitive transducer electrode to induce resonator vibration in the direction perpendicular to the substrate. A DC actuation voltage of 35V with 100 mV drive is applied to the moving part of the beam to create the necessary electrostatic for its movement and an AC signal is applied for the oscillation of the beam. The beam will show its oscillation with maximum amplitude at its resonance frequency. The resonance frequency of 7.7 MHz with quality factor of 1000 was yielded through the proposed resonator and this has potential suitability for high frequency mechanical filters.

Keywords: MEMS; High Frequency; Accelerometer; Actuation Voltage; Beam Structure; Mechanical Filter

1. Introduction

Since the past two decades, a multiple number of micro-electro-mechanical system (MEMS) devices have been developed and commercialized due to their ultra-low power consumption, higher thermal stability, reduce ageing effect, compact size and reduced cost as a direct consequence of batch fabrication technology [1, 2]. Significant advancements in the recent years have extended MEMS technology towards radio frequency, microwave and millimetres wave applications areas. There is a need for micro-machining and MEMS based systems for RF and microwave applications which are aroused from the inherent limitations of existing RF components and devices [3]. Especially, in the context of wireless communication the RF front end components like ceramic filters, quartz crystal, SAW filters and now FBAR filters which have the capability of achieving high Quality factor needed for RF and IF band pass filtering and frequency generation functions; they all off-chip components that must be interface with transistor function at the board level. These off-chip components not only lead to consumption of a sizable amount of the total board area but also increase the assembly cost of the components and devices. New advancements in vibrating RF micro-electro-mechanical system technology that have achieved on-chip resonators that could operate in GHz frequencies with Q's as high as of 10,000 may now not only provide a potential solution to the above problems, but might also enable a paradigm shift in transceiver design in which the advantages of high-Q (as in filters and oscillators)

* Corresponding author. *E-mail address: kurmendra.nits@gmail.com*

are addressed rather than suppressed [4, 5].

Radio frequency MEMS resonators find widespread applications in Analog systems such as RF filters, RF frequency mixers, RF oscillators, and duplexers, among others[6]. Due to their notably higher quality factor Q compared to other electrical counterparts, mechanical resonators are increasingly vital components in RF communication devices and circuits [7]. They offer a promising alternative to traditional quartz crystals as precise timing devices in oscillators for contemporary wireless data and communication applications. RF MEMS resonators boast compact dimensions, compatibility with integrated circuits, and cost-effectiveness.

As the frequency of integrated MEMS resonators increases, their size decreases. However, this reduction in size is accompanied by the emergence of non-linear behaviour, necessitating comprehensive analysis and understanding before practical application [8, 9]. The specific structure and layout of resonators dictate the nature of these nonlinearities, significantly impacting oscillator performance and thus requiring consideration for optimal resonator design. Therefore, it is crucial to model the dynamics of the resonator both numerically and experimentally to fully comprehend its response to frequency and other critical parameters.

The resonance frequency of fixed-fixed beam resonators was practically limited to 30 MHz, beyond which the quality factor decreased significantly. Higher resonant frequencies and quality factors were reported for micromechanical resonators with disk shapes due to their increased stiffness, enhancing power handling capacity compared to fixed-fixed beam resonators. A notable achievement was the demonstration of self-aligned vibrating radial-mode disk resonators with a record resonance frequency of 1.14 GHz and a quality factor exceeding 1,500 [10]. These resonators featured aligned stems for superior balancing, resulting in high quality factors not only in vacuum but also in air. Additionally, a hollow disk ring resonator was demonstrated, featuring a centralized support structure and notching at the support attachment to reduce support losses. This design led to the demonstration of a polycrystalline silicon resonator with a resonance frequency exceeding 1 GHz and a quality factor exceeding 10,000 [11]. Electrodes both inside and outside the disk ring structure enabled larger electrode overlap area, contributing to higher quality factors and lower impedances. Resonator structures suitable for UHF range RF applications require smaller size and higher stiffness to achieve large quality factors, although reducing size decreases power handling capacity. A radial-contour mode disk resonator structure was demonstrated to achieve high resonance frequency while retaining relatively larger dimensions, with a fundamental frequency of 433 MHz and a quality factor exceeding 4000[12]. Furthermore, a metal micro electromechanical resonator with a resonance frequency of nearly 60 MHz and a quality factor of about 54,507 was reported, utilizing nickel as a high-quality structural material for RF MEMS. Anchorless disk resonator designs supported by solid filling between the disk and electrodes achieved quality factors as high as 54,507 [13]. Additionally, a torsional mode silicon triangular beam resonator was demonstrated with a resonance frequency of 20 MHz and a high-quality factor of approximately 220,000, attributed to its low anchor loss and lower squeeze film damping compared to flexural mode vibration [14]. Such high-quality factor resonators offer higher frequency accuracy and lower power consumption. To study the microelectromechanical resonators, the researchers have been using finite element approaches with mesh [15, 16].In addition to conventional finite-element-based approaches, meshless methodologies have emerged as effective computational tools for the static and dynamic analysis of beam-like structures. The reproducing kernel particle method (RKPM), for example, has been employed to investigate the dynamic response of beams while considering both linear and nonlinear beam formulations [17]. The meshless local Petrov–Galerkin (MLPG) method combined with generalized moving-least-squares interpolation has also been developed for fourth-order thin-beam problems, enabling derivative information of the field variable to be incorporated directly into the approximation scheme [18]. Meshless formulations have further been extended to nanoscale vibration problems. A nonlocal meshless approach has been employed for the flexural vibration analysis of double-walled carbon nanotubes with arbitrary boundary conditions [19], while RKPM-based meshless formulations combined with nonlocal Rayleigh, Timoshenko, and higher-order beam theories have been applied to the free-vibration analysis of elastically embedded single-walled carbon nanotubes [20]. Related studies have also demonstrated the importance of advanced beam theories in describing beam-like structures under complex loading and size-dependent conditions. Timoshenko beam theory has been employed to investigate the impact response of functionally graded carbon-nanotube-reinforced composite beams under thermal environments [21], while Euler–Bernoulli, Timoshenko, and higher-order beam theories incorporating surface-energy effects have been used to investigate thermoelastic buckling of tapered nanowires [22]. These studies demonstrate the broad applicability of meshless and higher-order beam formulations from macro- to nanoscale structural problems. Nevertheless, the finite element method is adopted in the present work because it enables convenient implementation of the coupled structural and electrostatic physics of the proposed MEMS resonator within the COMSOL Multiphysics framework.

2. Nomenclature

L	Length of the resonator beam

d Depth of the resonator beam
h Height of the resonator beam
k Spring constant
Si_3N_4 Silicon Nitride
Si Silicon

3. Quantitative Description of Micromechanical Resonator

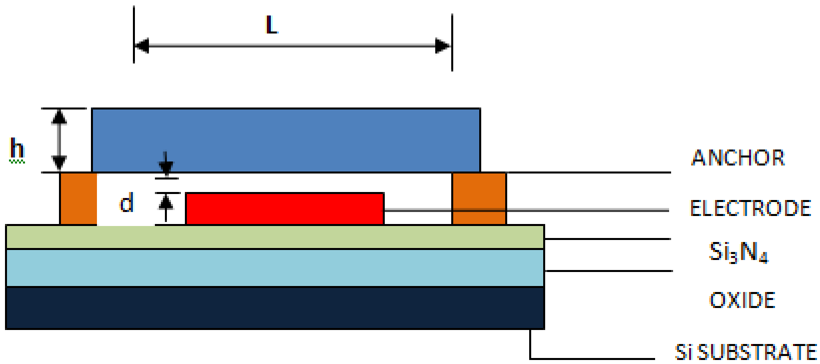

Fig 1: Perspective view of a schematic of Double-Clamped beam Resonator

The above Fig. 1 shows a fixed-fixed beam or double clamped beam micromechanical resonator. The resonator beam is suspended above the substrate and the conductive strip underlying the center of the resonator served as capacitive transducer electrode to induce resonator vibration in the direction perpendicular to the substrate. Here the resonator structure can be viewed as composed of two parts – the moving part which is the resonator beam, and the fixed part which is the underlying electrode. Here the moving and the fixed part of the resonator structure forms two electrodes of a capacitor. A DC actuation or pull-in voltage is applied to the suspended movable part of the beam electrode and an AC signal to the bottom fixed electrode. The DC voltage is applied to cause the necessary electrostatic force which is necessary for the movement of the beam and cause actuation. The electrostatic force will bend the beam in the downward direction in z-direction but the beam will oscillate only if this force oscillates, which is done by applying an AC signal at the fixed electrode which remains integral part of the resonator structure. The beam oscillates with the maximum amplitude at the resonance frequency given by the expression [23-25]

$$\omega = \sqrt{\frac{k}{m}} \tag{1}$$

where, k is the spring constant and m is the effective mass of the beam.

In order to maximize the resonant frequency, the effective resonator stiffness or the spring constant, k must be maximized while effective mass, m must be minimum. The resonant frequency depends upon many factors including geometry, structural material properties, stress, the magnitude of the applied DC bias, and the surface topology. Accounting these factors while neglecting the finite width effects, the resonance frequency can be written as [26]

$$\omega_0 = \omega_{nom}(1 - g(d, Vp))^2 \tag{2}$$

The function $g(d,V_p)$ represents the normalized contribution of the voltage-dependent electrical stiffness to the resonance frequency. Consistent with Eq. (2), it is defined as

$$g(d, V_p) = 1 - 1\left[1 - \frac{k_e(d, V_p)}{k_m}\right]^{\frac{1}{4}} \tag{3}$$

where k_m is the mechanical stiffness of the resonator and $k_e(d,V_p)$ is the magnitude of the negative electrostatic stiffness. Under the parallel-plate approximation, the electrostatic force is expressed as

$$F_{es} = \frac{\varepsilon_0 A V_p^2}{2(d - w_0)^2} \tag{4}$$

and the corresponding electrostatic stiffness is obtained from the force gradient as

$$ke(d,Vp) = \left(\frac{\partial Fes}{\partial w}\right)\bigg|_{w=w_0} = \frac{\varepsilon_0 A V_p^2}{(d - w_0)^3} \tag{5}$$

where ε_0 is the permittivity of free space, A is the effective electrode overlap area, d is the initial beam–electrode gap, w_0 is the equilibrium displacement under the applied DC bias, and V_p is the applied DC bias voltage. Accordingly, Eq. (2) can equivalently be written as

$$\omega_0 = \omega_{nom}\sqrt{\left[1 - \frac{k_e(d,V_p)}{k_m}\right]} \tag{6}$$

This relation explicitly demonstrates the electrostatic spring-softening effect: an increase in the applied DC bias increases the magnitude of the negative electrostatic stiffness, thereby reducing the effective stiffness and consequently shifting the resonance frequency downward. The $\omega_{nom}$is represented by

$$\omega_{nom} = 1.03k\sqrt{\frac{Eh}{\rho L^2}} \tag{7}$$

Where, ω_{nom} is the nominal mechanical resonance frequency of the resonator when there was no applied voltage. g is the function that models the effects of an electrical stiffness k_e that appears when electrodes and voltages are introduced and that excludes the mechanical stiffness and κ is the scaling factor which modes the effects of the surface topology. According to the equation for resonant frequency, the resonance frequency increases as the length decreases. The oscillation of the beam changes the gap d between electrodes also changing the capacitive between the two electrodes. The variation in the capacitance will produce an AC current which can be given by [13]

$$i = V_p \frac{dC}{dt} \tag{8}$$

4. Mechanical Modelling of Micromechanical Resonator

This section describes the mechanical modeling of a double-clamped beam micromechanical resonator, commencing with an examination of the beam's displacement characteristics.

4.1. Displacement of Beam Under Weight

If the geometrical dimensions, the material parameters of the beam and the external force and the boundary condition are known, the displacement function ω(x) of the beam having length L, breadth b and height h, can be found using below equation [23]

$$-E.I.w^{"}(x) = \frac{M_b g x}{2} - \frac{M_b g x^2}{2L} - m_0 \tag{9}$$

Where, E is Young's modulus of the beam material, I is the moment of inertia of the beam and Mb is the total mass of the beam. The boundary conditions are

$$\omega(0) = 0, \omega^{'}(0) = 0, \omega(L) = 0 \text{ and } \omega^{'}(L) = 0 \tag{10}$$

$$m_0 = \frac{\rho g b h L^2}{2L} \tag{11}$$

The displacement function of the beam is [23]

$$\omega(x) = \frac{M_b g}{24ELI} x^2 (L-x)^2 = \frac{\rho bhgx^2}{2Eh^2} \tag{12}$$

Therefore, the maximum displacement at the center of the beam; at x=L/2 is [9]

$$\omega_{\max} = \frac{\rho g L^4}{32Eh^2} \tag{13}$$

4.2 Vibration Frequencies of a double clamped beam

The linear partial differential equation governing the vibration of the beam is given as [9]

$$EI\frac{d^4\omega}{dx^4} + \rho A\frac{d^2\omega}{dt^2} = q(x) \tag{14}$$

If there is no loading on the beam then,

$$EI\frac{d^4\omega}{dx^4} + \rho A\frac{d^2\omega}{dt^2} = 0 \tag{15}$$

The general solution to the equation (11) can be considered as the superposition of the different vibration modes [23]i.e.,

$$\omega(x,t) = \sum_n W_n \frac{x}{L}(A_n \operatorname{Cos}\omega_n t + B_n \operatorname{Sin}\omega_n t) \tag{16}$$

Where, ω_n is the radial frequency and Wn is shape function of the nth vibration mode. By substituting equation (12) in equation (11) and using dimensionless variable η = x/L, the equation for Wn (η):

$$W''(\eta) - \frac{\rho A}{EI} L^4 \omega_n{}^2 W_n(\eta) = 0 \tag{17}$$

Let

$$(k_n)^4 = \rho A L^4 \frac{\omega_n{}^4}{EI} \tag{18}$$

We have

$$W''_n(\eta) - k_n{}^4(\eta) = 0 \tag{19}$$

By using $W_n = e^{n\lambda}$ as a trail solution we have

$$\lambda^4 - k_n{}^4 = 0 \tag{20}$$

The solutions to the equation are $\lambda = k_n, -k_n, ik_n, -ik_n$. Therefore, the general form of the shape is

$$W_n(\eta) = Ae^{k_n\eta} + Be^{-k_n\eta} + Ce^{ik_n\eta} + De^{-k_n\eta} \tag{21}$$

By substituting the boundary conditions, the equations for A,B,C and D are

$$\begin{bmatrix} 1 & 1 & 1 & 1 \\ k_n & -k_n & ik_n & k_n \\ e^{k_n} & e^{-k_n} & e^{ik_n} & -ie^{ik_n} \\ k_n e^{k_n} & k_n e^{-k_n} & ik_n e^{ik_n} & -ik_n e^{-ik_n} \end{bmatrix} \begin{bmatrix} A \\ B \\ C \\ D \end{bmatrix} = 0 \tag{22}$$

For non-trivial solutions, the determinant of the matrix in the equation (22) must be zero.

$$\begin{vmatrix} 1 & 1 & 1 & 1 \\ k_n & -k_n & ik_n & k_n \\ e^{k_n} & e^{-k_n} & e^{ik_n} & -ie^{ik_n} \\ k_n e^{k_n} & k_n e^{-k_n} & ik_n e^{ik_n} & -ik_n e^{-ik_n} \end{vmatrix} = 0 \tag{23}$$

The equation (17) can be reduced to a simple equation as

$$\mathrm{Cosh}(k_n).\mathrm{Cos}\, k_n - 1 = 0 \tag{24}$$

This result indicated that the eigen values, k_n for the shape function must satisfy the above equation. Some k_n values found from this equation are

$$k_1 = 1.875, k_2 = 4.694, k_3 = 14.137, k_6 = 17.279$$

Thus, the radial frequency of the fundamental vibration mode is

$$\omega_1 = \frac{(1.875)^2}{L^2}\sqrt{\frac{EI}{\rho A}} = 1.015\frac{h}{L^2}\sqrt{\frac{E}{\rho}} \tag{25}$$

5. Design and Simulation

5.1 Eigen Frequency Analysis of Micromechanical Resonator

ModelDescription:

A double clamped micromechanical resonator is modelled which is suspended above silicon substrate using two anchors at both ends of the polysilicon beam. Since we are analyzing the fundamental vibration frequencies of the resonator, we do not need any actuation or biasing. COMSOL Multiphysics solve the Eigen frequencies and Eigen values automatically by solving the differential equations of the beam.

Table 1: Geometricspecification ofthedoubleclampedbeamresonator.

Sl. No.	Parameters	Values (in um)
1	ResonatorLength	L=40
2	ResonatorWidth	W=8
3	ResonatorHeight	H=2
4	Gapbetweenbeamandfixedelectrode	d =0.25

The geometrical dimensions of the beam resonator are given in the Table 1 and the materials properties for the materials which were utilized during the studies have been given in Table 2.

The simulation of designed resonator in normal mode is done using COMSOL Multiphysics and eigen frequency at normal mode is obtained as 10.16 MHz as shown in Fig. 2 which is considered ideal for high frequency applications such as mechanical filters, and other wireless applications.

Table 2: MaterialPropertiesof the doubleclampedbeamresonator.

Component	Material	Material's Properties	Value	Unit
	Polysilicon	RelativePermittivity	4.5	1

Resonator		CoefficientOfThermal Expansion	2.6e-6	1/K
		HeatCapacity atConstantTemperature	678	J/kgK
		Density	2320	Kg/m³
		ThermalConductivity	34	W/mK
		Young'sModulus	160e9	Pa
		Poisson's Ratio	0.22	1
Environment	Air	RelativePermittivity	1	1

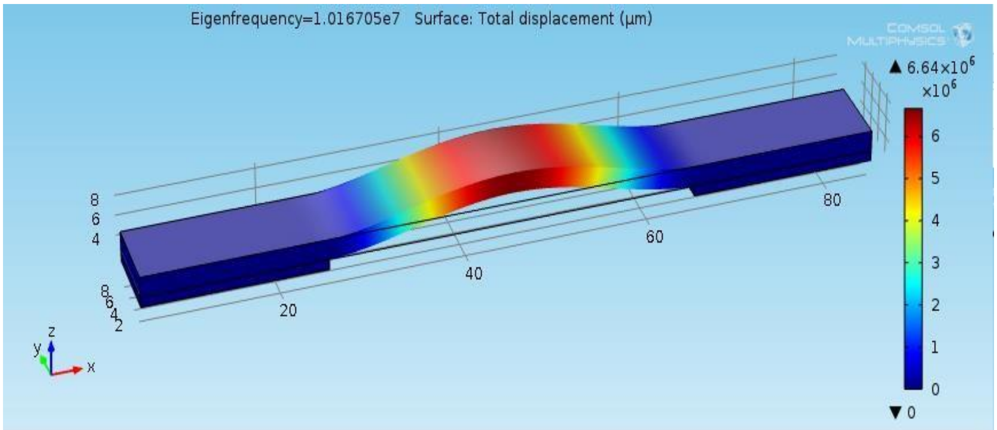

Fig 2: Eigen frequency of the resonator in normal mode

5.2 Stationary analysis of the micromechanical resonator

In the analysis of the stationary state of the silicon-based resonator, the wafer beneath is grounded using a ground terminal under Electrostatic(s) module, and a 35V electrostatic voltage is applied to the driving electrode using the same module. The polysilicon is considered as an ideal conductor, which allows the bias voltage to spread across all external surfaces of the resonator and its anchors, serving as a potential boundary condition. Figure 3 presents the meshing model of the designed resonator, while Figure 4 illustrates the structural deformations. These results are obtained using COMSOL Multiphysics software after applying the bias voltage. In the solid mechanics simulations, silicon oxide and silicon nitride are treated as rigid materials, providing support to the structure at the base of its electrode, and these regions are excluded from the solid mechanics equations.

In a vacuum or other medium, the forces between charged bodies are calculated by assuming a hypothetical state of stress within the field. The electromagnetism or Maxwell stress tensors are employed to determine the stresses induced in the material due to an electric field, as well as the surface forces acting on bodies in air or vacuum [27, 28]. This model presumes that the polysilicon is heavily doped, allowing it to be considered a perfect conductor. It is assumed that the electric field within the resonator is zero, which means the Maxwell stress tensor is also zero inside the material, resulting in no volumetric electrical forces within it. The Maxwell stress tensor in the medium surrounding the resonator structure, where the electric field is not zero, is represented by [29]

$$T_{EM,V} = -\frac{1}{2}(E.D)I + ED^{T} \tag{26}$$

A net force on the surface typically results from the discontinuity of the stress tensor at the interface. However, because it is undesirable to apply a stress term throughout the vacuum, the force is only computed on the surface of the resonator and is applied by electromechanical interface node. The surface force can be given by

$$n_1 T_{EM,V} = -(\frac{1}{2}E.D)n_1 + (n_1 E)D \tag{27}$$

Where, n_1 is surface normal pointing out from the mechanical body.

Fig 3: Model Meshing

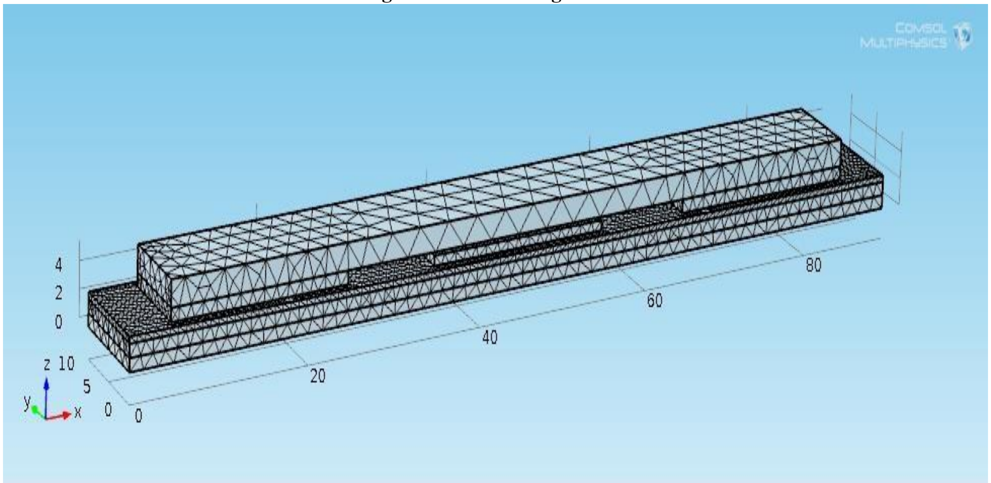

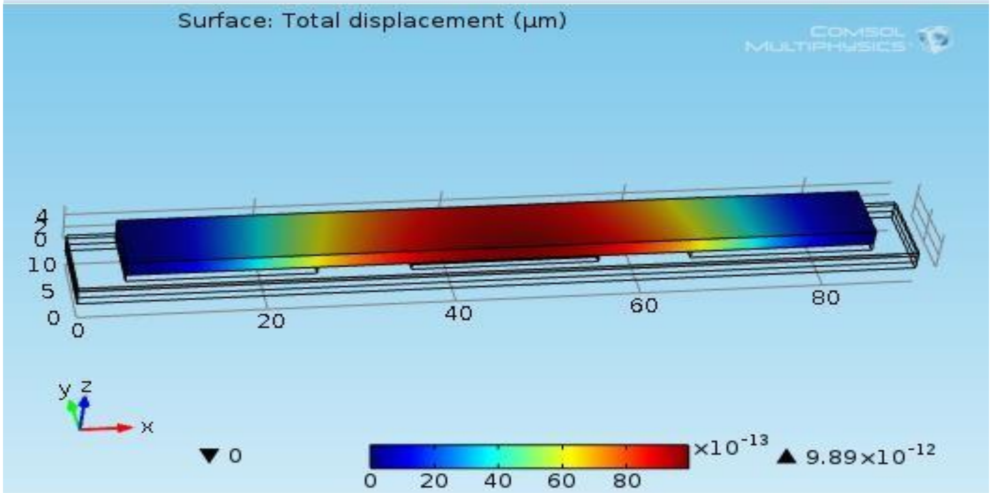

Fig 4: Biased Resonator structure without air environment

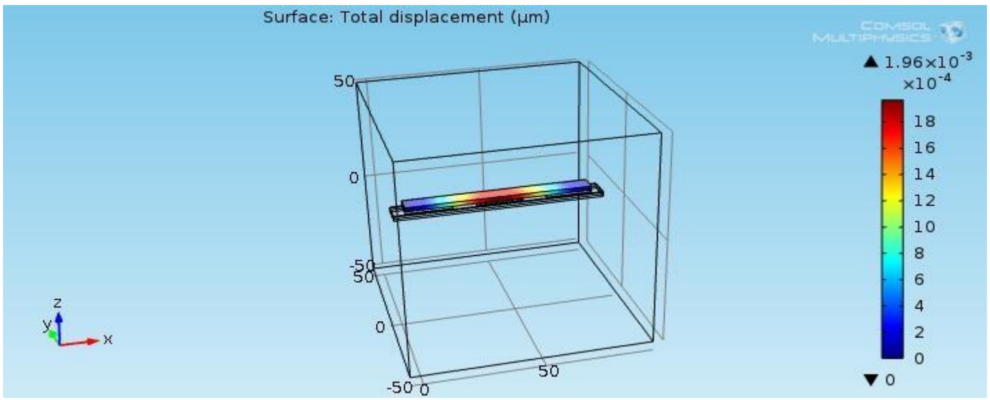

Fig 5: Biased Resonator structure within air environment

The above Figure. 4 shows the displacement of the structure with an applied DC bias. The structural displacement is maximal on the symmetry plane at the center of the device as expected. The maximum displacement is 16.1 nm. The electrostatic potential isosurfaces are also shown in Figure.5 as the case remains, the isobars are uniformly distributed and it is closest together between the resonator and electrode. This corresponds to a region of uniform electric field in the device [23]. The fringing fields can also be seen around the electrode. Here the surface of the resonator is assumed to be perfectly grounded which is a result of the potential boundary conditions used and it is equivalent to the assumption made that polycrystalline silicon is a perfect conductor.

5.2.1 Validation of the Perfect-Conductor Approximation

The finite electrical conductivity of doped polysilicon was considered to assess the validity of the equipotential-conductor approximation employed in the electrostatic model. The characteristic charge-relaxation time is expressed as

$$\tau c = \frac{\varepsilon_0 \varepsilon_r}{\sigma} \tag{28}$$

where ε_0 is the vacuum permittivity, εr is the relative permittivity, and σ is the electrical conductivity of polysilicon. For the adopted values εr = 4.5 and σ = 5 × 10^4 S/m, the charge-relaxation time is 7.97 × 10^{-16} s. In comparison, the characteristic mechanical timescale at the simulated resonance frequency fr = 7.706 MHz is

$$\tau m = \frac{1}{\omega_r} = \frac{1}{2\Pi f_r} = 2.07x10^{-8}s \tag{29}$$

$$\frac{\tau_c}{\tau_m} = 3.86x10^{-8} \ll 1 \tag{30}$$

As shown in Fig. 6, the conductivity sensitivity analysis over 10^3–10^6 S/m further shows that the charge-relaxation time remains several orders of magnitude smaller than the characteristic mechanical timescale throughout the investigated range. This large separation of electrical and mechanical timescales indicates rapid charge redistribution within the doped-polysilicon resonator relative to its mechanical response and therefore supports the equipotential-conductor approximation at the operating frequency.

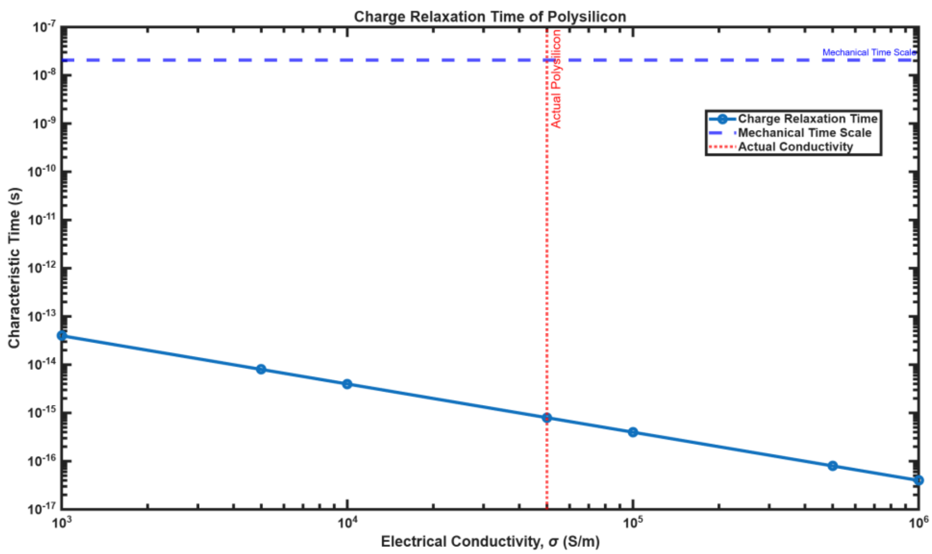

Fig. 6: Conductivity-dependent charge-relaxation time of the polysilicon resonator compared with the characteristic mechanical timescale 1/ω_r at f_r = 7.706 MHz. The adopted polysilicon conductivity is 5 × 10^4 S/m.

5.3. Frequency response analysis of micromechanical resonator

For the frequency domain analysis of the proposed resonator, an applied drive voltage consisting of a 35V DC with a 100-mV drive signal added as a hormonic perturbation [30]. To obtain the response of the system, we must add a damping to the model. For this study it is assumed that the damping mechanism is Rayleigh damping or material damping. Specific damping requires two material constants αdM and βdK. For a system with a single degree of freedom, the equation of the motion with viscous damping is given by

$$m\frac{d^2u}{dt^2}+C\frac{du}{dt}+ku=f(t) \tag{31}$$

Where c is the damping coefficient, m is the mass, k is the spring constant, u is the displacement, t is time and $f(t)$ is a driving force. In Rayleigh damping model, the parameter c is related to the mass m and stiffness k by the equation

$$c=\alpha dM*m+\beta dK*k \tag{32}$$

The Rayleigh damping term in COMSOL Multiphysics is proportional to the mass and stiffness matrices which are added to the static weak term. The damping coefficient c is generally defined as a damping ratio or factor which is expressed as a fraction of the critical damping c0. The damping factor ξ is given by

$$\xi=\frac{c}{c_0} \tag{33}$$

where for a system with one degree of freedom

$$c_0=2\sqrt{km} \tag{34}$$

Finally for the larger value of quality factor, Q we have

$$\xi=\frac{1}{2Q} \tag{35}$$

The material parameters αdM and βdK are usually not available in the literature. Often the damping ration is available, typically expressed as a percentage of the critical damping. It is possible to transform damping factors to Rayeigh damping parameters. The damping factor ξ for a specified pair of Rayeigh Parameters, αdM and βdK, at the frequency, f, is given [31]

$$\xi=\frac{1}{2}(\frac{\alpha dM}{2\pi f}+\beta dK*2\pi f) \tag{36}$$

using this relationship at two frequencies, f_1 and f_2 with different damping factors ξ_1 and ξ_2 results in an equation system that can be solved for αdM and βdK

$$\begin{bmatrix}\frac{1}{4\pi f_1} & \pi f_1\\ \frac{1}{4\pi f_2} & \pi f_2\end{bmatrix}\begin{bmatrix}\alpha dM\\ \beta dK\end{bmatrix}=\begin{bmatrix}\xi_1\\ \xi_2\end{bmatrix} \tag{37}$$

The damping factors for this model are provided as αdM = 4189 Hz and $\beta dK=8.29*10^{-13}$ s consistent with the observed quality factor of 8000 for the fundamental mode. The Rayleigh damping coefficients αdM and βdK are employed as effective proportional damping parameters and are not regarded as intrinsic material constants of polysilicon. Their suitability was verified at the fundamental resonant frequency of the proposed beam (fr = 7.706 MHz). Using αdM = 4189 s^{-1} and βdK = 8.29 × 10^{-13} s, the Rayleigh relation

$$\zeta=\frac{1}{2}\left(\frac{\alpha dM}{\omega_r}+\beta dK\omega_r\right) \tag{38}$$

gives ζ = 6.33 × 10^{-5}, corresponding to Q ≈ 7895, which is close to the adopted target modal value of approximately 8000. This frequency range is also physically relevant to polysilicon flexural resonators; Srikar and Senturia [32]reported a Zener thermoelastic damping critical frequency of approximately 7 MHz for representative fine-grained polysilicon beams and demonstrated consistency of the model with experimental quality-factor data. Therefore, the adopted Rayleigh coefficients are interpreted as effective parameters for representing the prescribed modal damping near the operating frequency rather than as experimentally determined damping constants of polysilicon.

Figure 7 shows the frequency response of the resonator which the maximum displacements of the resonator beam as a function of frequency. The quality factor Q above plot can be estimated as [8, 9]

$$Q = \frac{f_0}{bandwidth} \tag{39}$$

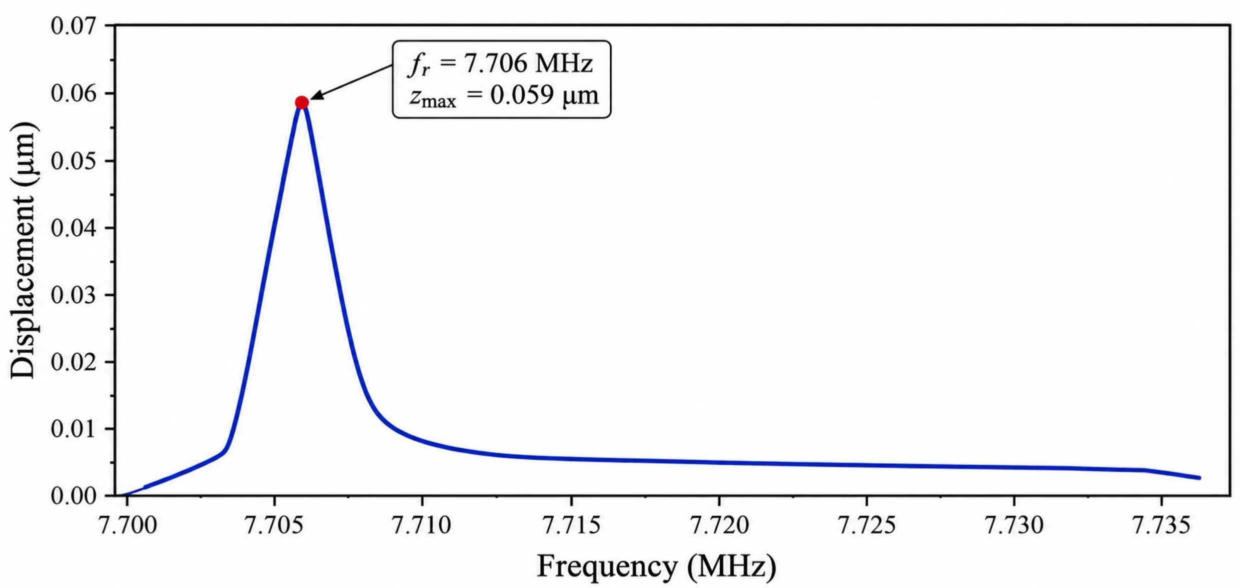

Fig 7: Frequency response of the fundamental mode of the resonator

The frequency-response analysis yields an effective quality factor of approximately 1000 for the considered air-damped condition. Higher Q-factors are generally expected under reduced-pressure conditions due to the reduction in fluid-related energy dissipation. It should be noted that the air-environment response considered here employs an effective damping representation and does not explicitly resolve squeeze-film damping within the narrow beam–substrate gap. Squeeze-film damping can be a significant dissipation mechanism in MEMS structures with small gaps and is generally described using Reynolds-equation-based fluid-film models [33]. Therefore, the Q≈1000 case considered here should be interpreted as an effective air-damped numerical case used to examine the influence of increased damping on the frequency response, rather than as a quantitative prediction of the squeeze-film-limited Q-factor. Explicit squeeze-film/fluid–structure modelling would be required for quantitative prediction of air-induced energy dissipation.

6. Comparison of analytical and simulated performance of the Micromechanical Resonator

6.1 Effect of beam length L on Eigen frequency

The designed resonator model is simulated using COMSOL Multiphysics software and Figure 8-12 is showing the variation of eigen frequencies for the change in resonator beam length. From the result it is visible that eigen frequency progressively seen decreasing when the length of the beam is increased which is mathematically supported by equation 25. The reason behind reduction in the eigenfrequency is due to reduction in effective flexural stiffness of the resonator as its length increases. If was consider a beam with fixed cross-sectional geometry, the bending stiffness is inversely proportional to cube of the beam length. Simultaneously, the effective mass of the beam keeps increasing with increase in its length.

Eigen frequency analyses are validated by varying the length of the resonator beam L and the resonator height h. the effect of beam length L on Eigen frequency is shown in the figures

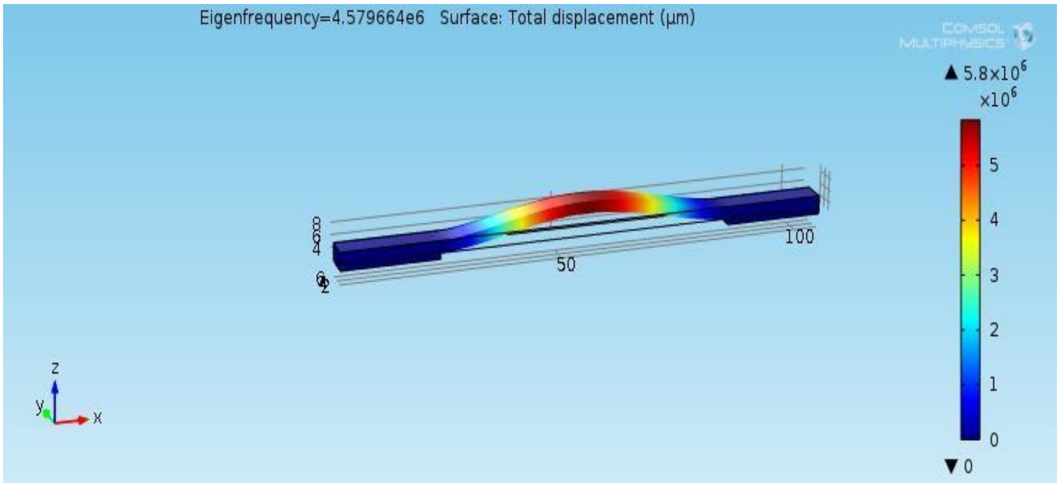

Fig 8: Eigen frequency of camped clamped resonator for L = 30 µm

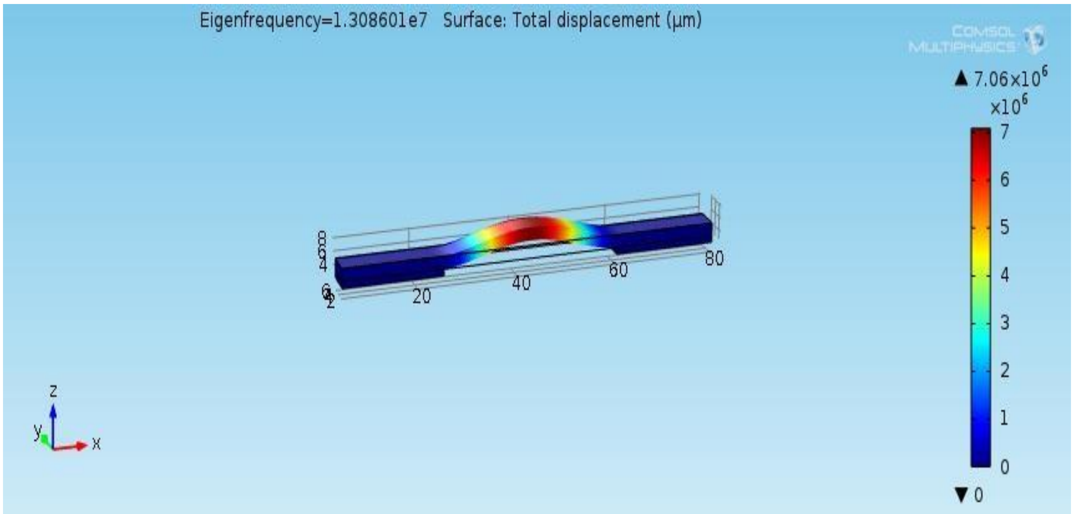

Fig 9: Eigen frequency of camped clamped resonator for L = 35 µm

The natural frequency of the beam resonator is proportional to the square root of the ration of spring constant of the beam material to the effective mass of the beam resonator. Therefore, an increase in the beam length results in significant decrease in the resonator spring constant or stiffness and thus, lowers it eigenfrequency[34]. The other reason is that a longer beam remains more flexible and so requires comparatively less restoring force to undergo vibrations, resulting in much lower resonant frequency. And therefore, the flexural vibrational characteristics of a double clamped beam resonator is dependent of eigne frequencies and beam length of the resonator.

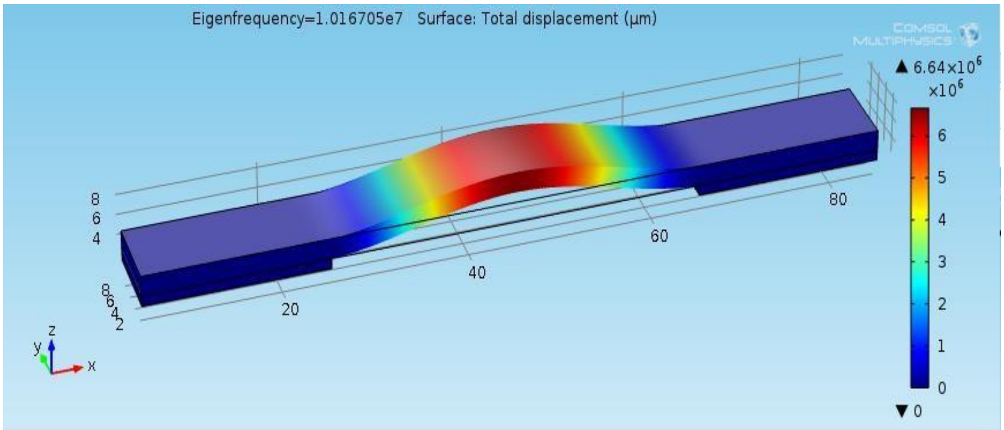

Fig 10: Eigen frequency of camped clamped resonator for L = 40 µm

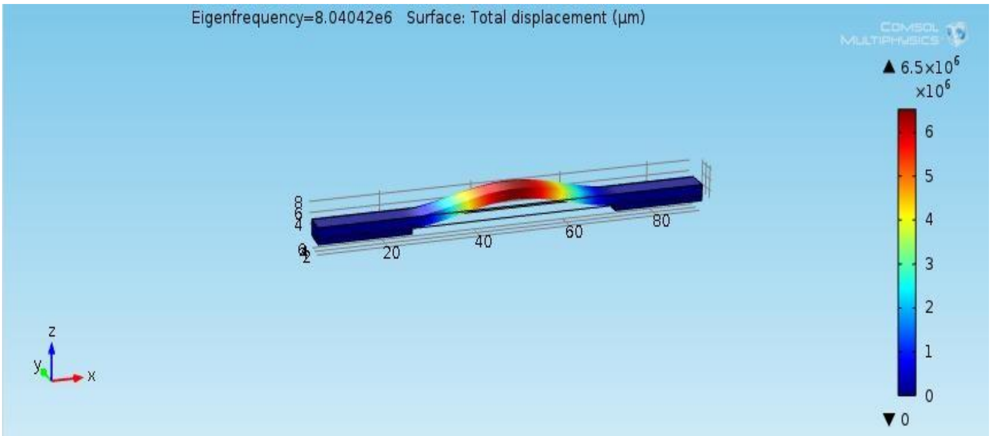

Fig 11: Eigen frequency of camped clamped resonator for L = 45 µm

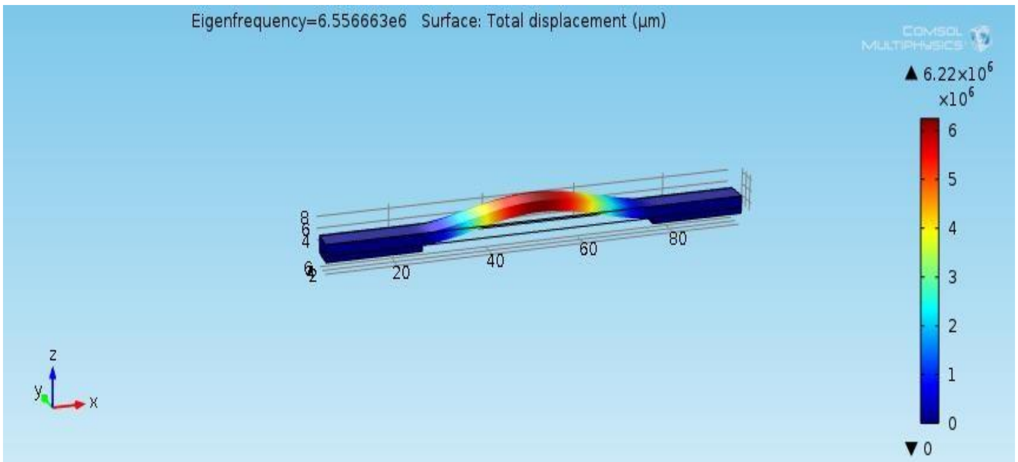

Fig 12: Eigen frequency of camped clamped resonator for L = 40 µm

Table 3: Comparison between simulated and analytical Eigen Frequency for different Length.

Resonator length (in µm)	Simulated Eigen Frequency (in MHz)	Analytical Eigen Frequency (in MHz)	% Error
30	17.00	18.00	5.55
35	13.00	13.76	5.52
40	10.16	10.05	1.09
45	8.04	8.32	3.36
50	6.55	6.74	2.81

The simulated Eigen frequencies and the analytical Eigen frequencies are very close.

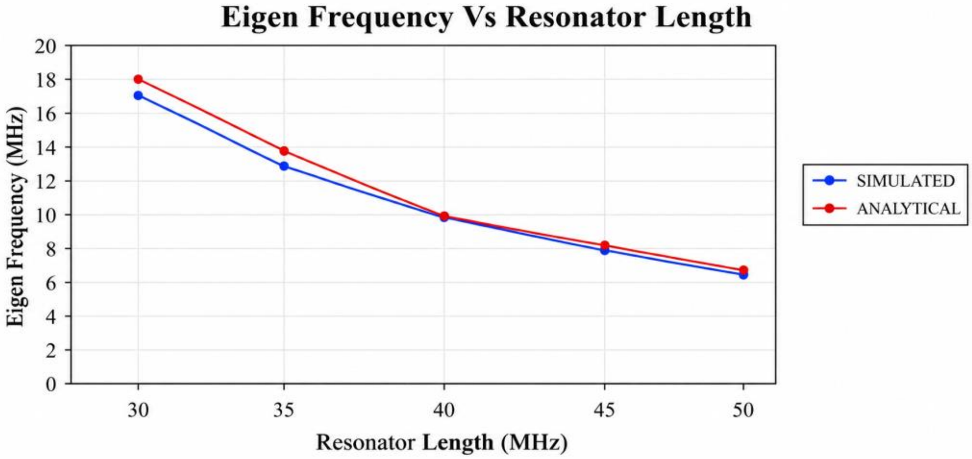

Fig 13: Eigen Frequency Vs Resonator Length Plot

Figure 13 shows the inverse relation between Eigen frequency and the resonator beam length. From Table 3, It is also clear that the simulated Eigen frequencies and the analytical Eigen frequencies are very close.

6.2 Effect of beam height h on Eigen frequency:

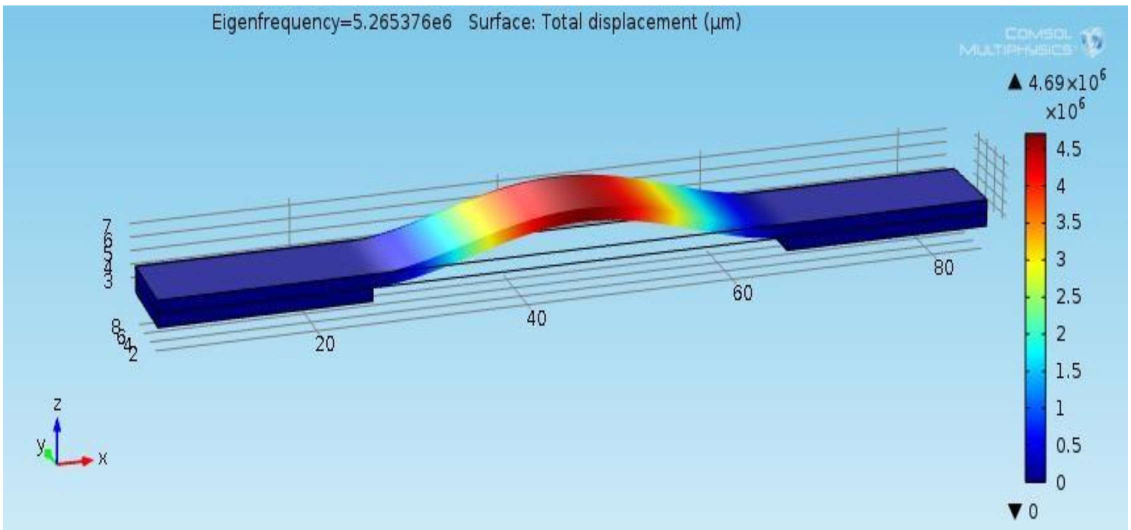

Fig 14: Eigen frequency at h = 1 µm

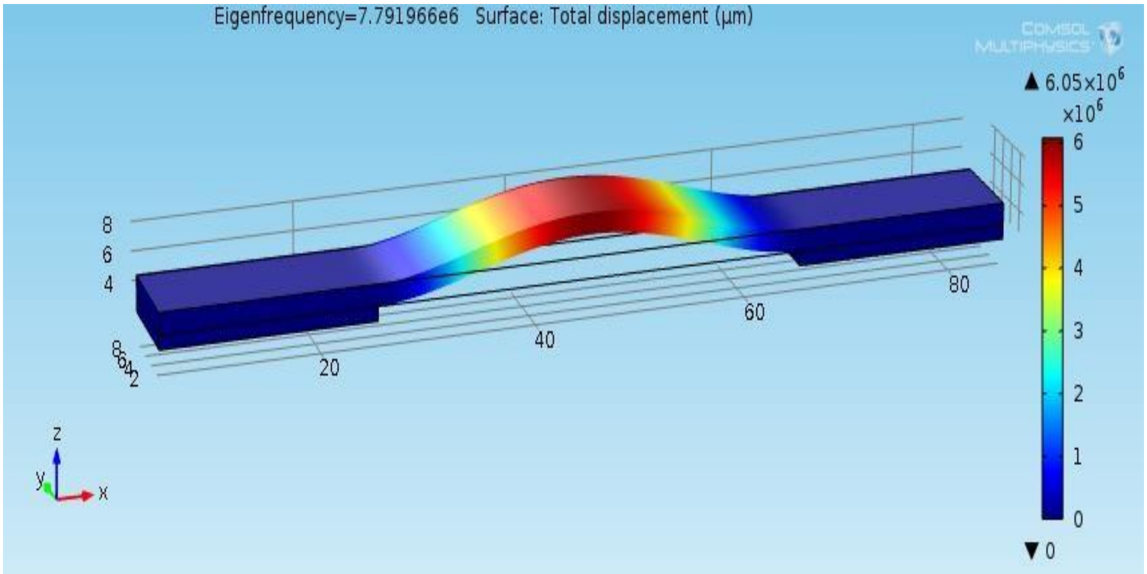

Fig 15: Eigen frequency at h = 1.5 μm

The next study was performed to see the impact of varying height of the resonator and the results are presented in the Figure 14-18. The increase in the resonator beams high resulted in increasing eigen frequencies as per model equation (19) and also analytical result presented in Table 4 confirm this effect. The primary reason is that the increasing height of the resonator attributed in increased flexural stiffness of the beam resonator[35]. As the shape of the beam of the resonator is of rectangular in shape and for rectangular beam moment of inertia is cubic related to its height which indicates that increasing height increases moment of inertia consequently flexure stiffness increases. Further, the effective mass of the resonator increases with increment in the height of the resonator and the impact of increases stiffness also shows dominant effect on the dynamic response of the beam[36].

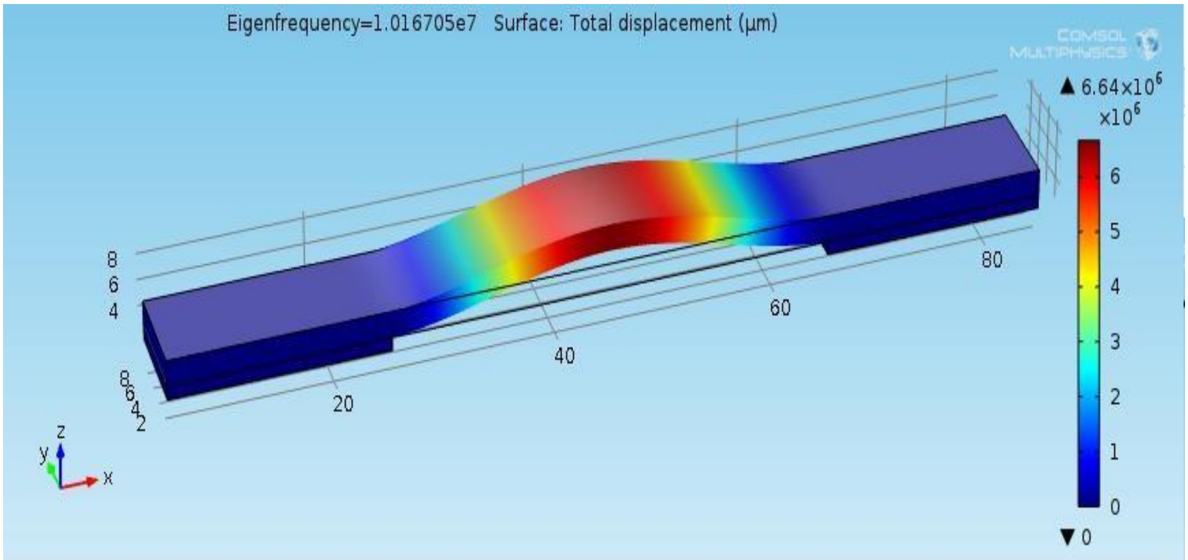

Fig 16: Eigen frequency at h = 2 μm

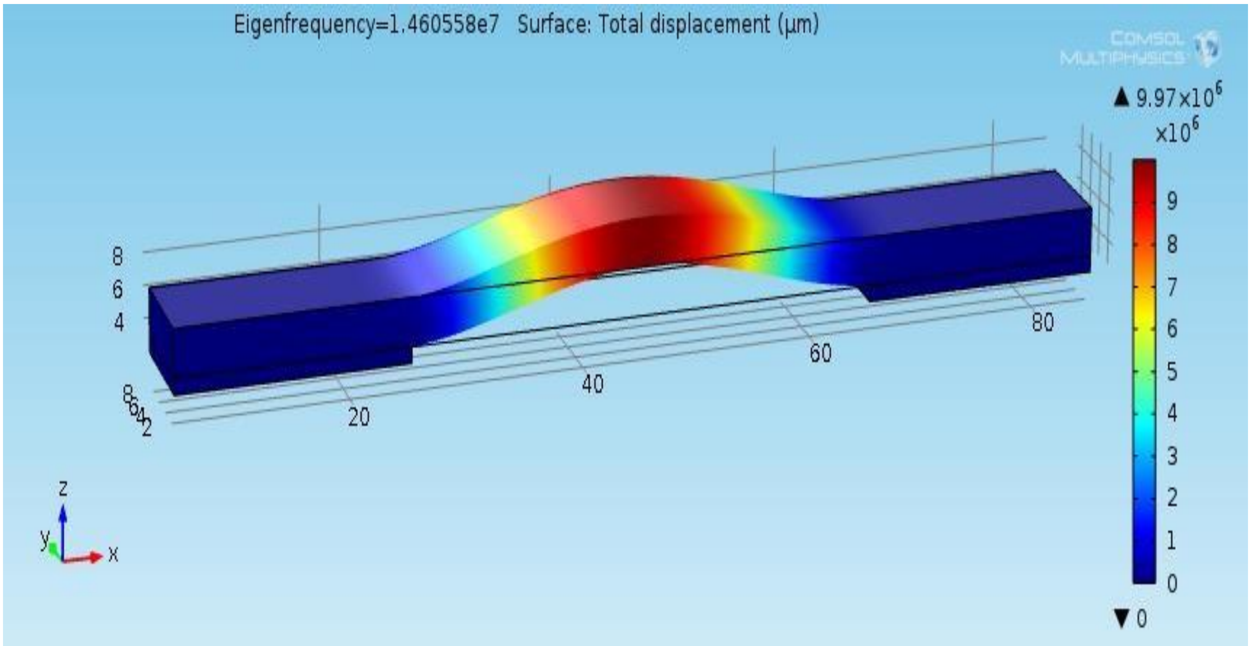

Fig 17: Eigen frequency at h = 2.5 µm

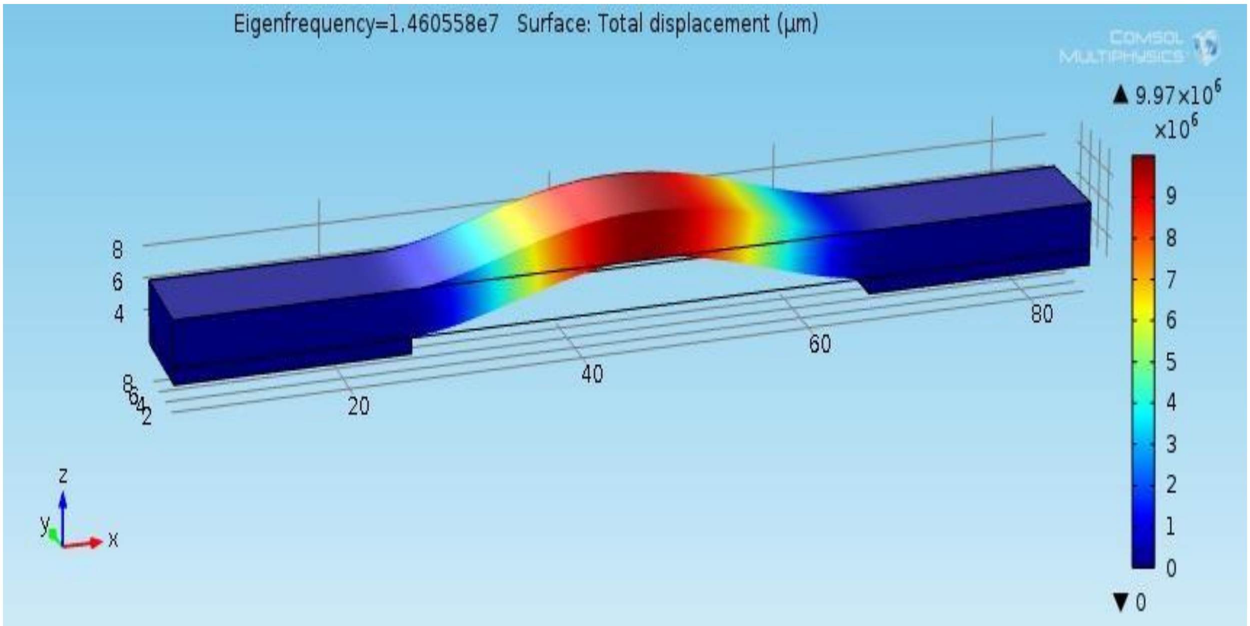

Fig 18: Eigen frequency at h = 3 µm

The analytical and simulated eigen frequencies exhibit close agreement for the relatively slender resonator configurations. For the fixed resonator length of 40 µm, increasing the height from 1 to 3 µm decreases the slenderness ratio L/h from 40 to 13.33. The deviation remains small for the slenderer configurations but increases to 5.69% at h = 2.5 µm and 8.10% at h = 3 µm. This increasing discrepancy can be attributed to the limitations of the classical Euler–Bernoulli formulation used in the analytical model. As the beam becomes relatively thicker, transverse shear deformation and rotary inertia, which are neglected in the Euler–Bernoulli formulation, become increasingly relevant. Consequently, the analytical formulation becomes less representative of the thickness-dependent flexural behaviour, whereas the 3D FEM model provides a more comprehensive representation of the structural response.

Table 4: Comparison between simulated and analytical Eigen Frequency for different height.

Resonator Height (in μm)	Simulated Eigen Frequency (in MHz)	Analytical Eigen Frequency (in MHz)	% Error
1.0	5.26	5.26	0.00
1.5	7.79	7.90	1.39
2.0	10.16	10.05	1.09
2.5	12.42	13.17	5.69
3.0	14.60	15.80	8.10

Figure 19 shows the relation between Eigen frequency and the resonator beam length. It is also clear that the simulated Eigen frequencies and the analytical Eigen frequencies are very close.

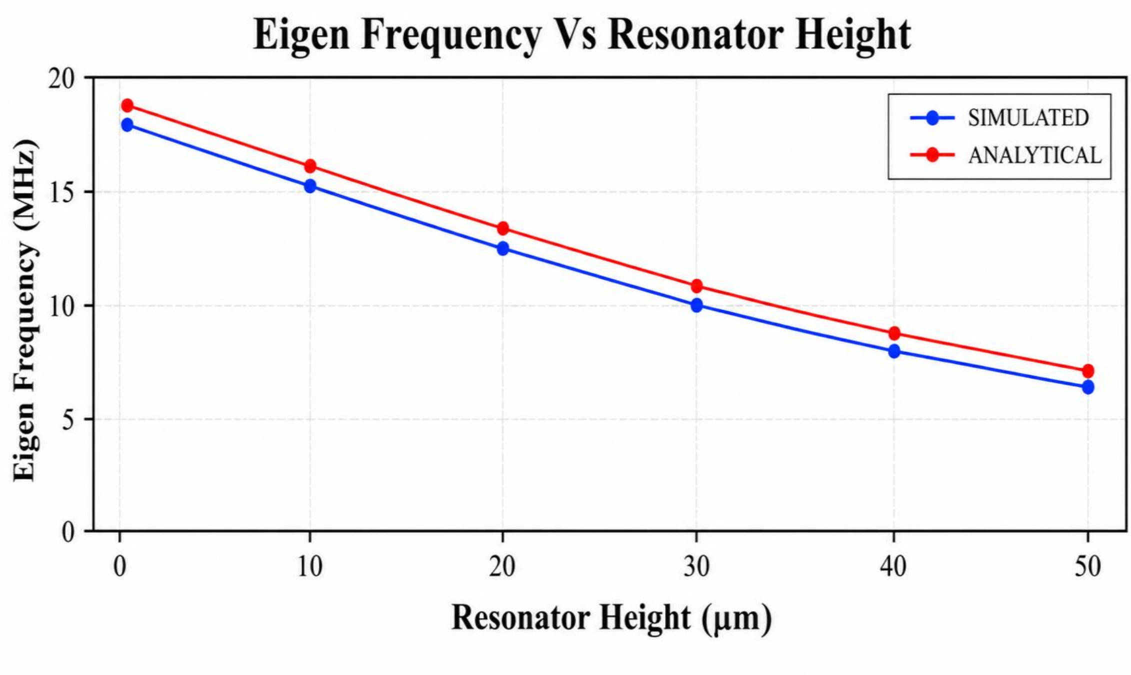

Fig 19: Eigen Frequency Vs Resonator Height Plot

6.1 Maximum displacement of the resonator

As seen in Figure 4 and Figure 5 maximum displacement of the resonator structure is 0.00989 nm or 9.89 pm in no environment condition and it is 1.96 nm in air environment with relative permittivity of 1.

Table 5: Effect of Environment around the resonator structure.

Environment	Simulated Maximum Displacement of the beam (in nm)
No environment	0.00989
Air environment	1.96

7. Result and Discussion

The Design of RF MEMS double-clamped beam resonator was investigated and the resonant frequency of the resonator was modelled. The structure was designed in COMSOL Multiphysics using the process steps available that emulated the fabrication procedure for MEMS. The vibration frequencies and modes of the resonator model were studied in COMSOL Multiphysics. Eigen frequency plot in Figure 2 shows that the Eigen frequency of the resonator at normal mode is 10.16 MHz which is ideal for High Frequency range in RF wireless applications. Figure 5 shows the z displacement of the structure with an applied DC bias. The structural displacement is maximal on the symmetry plane at the centre of the device as expected. The maximum displacement is 1.96 nm. Figure 8 to Figure 12 showed the variation of Eigen frequency with varying resonator beam length which show that with increase in resonator beam length, Eigen frequencies decreases and Figure 14 to Figure 18 showed the variation of Eigen frequency with varying resonator beam height reveals that with increase in resonator beam height, Eigen frequencies increases. The stationary analysis of the biased resonator was also done. The biased resonator as expected has shown the highest displacement at the centre of the beam just above the underlying electrode with the application of bias voltage of 35 V. The maximum displacement of the biased resonator was 9.89 picometer when the resonator structure was not immersed inside the air medium. But when the structure was enclosed within an environment of air, the maximum displacement and the resonant frequency increased to 1.96 nm and 7.7 MHz respectively. For the frequency domain analysis of the structure an applied drive voltage consisting of a 35 V DC offset with a 100mV drive signal added as a harmonic perturbation. Figure 6 shows the frequency response of the resonator which the maximum displacements of the resonator beam as a function of frequency. The resonator structure could yield resonant frequency of 7.7 MHz with Q around 1000 which can be use in High Frequency Micromechanical Filters. A state of art comparison of proposed double clamped beam resonator performance with existing work in literature is presented in Table 6.

Table 6: Comparison of the proposed resonator with representative MEMS resonators reported in the literature.

Literature / Citation	Year	Resonator Type	Material	Resonance Frequency	Q-Factor	Study
Sang et al. [37]	2020	Double-clamped beam	GaN/Si	139–911 kHz	$>10^5$	Experimental
Kaisar, T. et al. [38]	2022	Multimode MEMS resonator	AlN/Si	10, 30, 65 MHz	18,600; 4,350; 4,230	Experimental
Mion et al. [39]	2023	Double-clamped magnetoelectric resonator	AlN/FeCoHf	~MHz/sub-MHz regime	143	Experimental
Niu et al. [40]	2024	Doubly-clamped beam	MEMS beam	Multiple coupled modes	—	Experimental + theoretical
Garofalo et al. [41]	2025	Double-clamped beam	3C-SiC/Si	312.20–318.07 kHz	624,400–636,150	Experimental + modelling
Wang et al. [42]	2004	Radial-contour disk	Polysilicon	1.14 GHz	>1500	Experimental
Present work	2026	Double-clamped flexural beam	Polysilicon	7.706 MHz	≈1000	Analytical + FEM

8. Conclusion

A RF MEMS double clamped resonator for high frequency mechanical filters has been proposed. The model was based on the process steps used in the fabrication of RF micromechanical resonator in HF micromechanical filters. Eigen frequency of the resonator at normal mode was 10.16 MHz which is ideal for high frequency range in RF wireless applications as well. The maximum displacement obtained was 1.96 nm. The variation of eigen frequency with varying resonator beam length and beam height shows that with the increase in resonator beam length, the eigen frequencies decreases and increase in resonator beam height, eigen frequency increases. The frequency response of the resonator, the maximum displacement of the resonator beam as a function of frequency was also studied. The resonator structure could yield resonant frequency of 7.7 MHz with Q around 1000 which can be used in high frequency micromechanical filters. The analytical model was in good agreement with FEM simulation model with an error of just 9.4%. the accuracy of the model can be increased by considering that the polysilicon resonator is a perfect conductor and the substrate was perfectly grounded.

References

[1] Y. J. Chen, Advantages of mems and its distinct new applications, *Advanced Materials Research,* Vol. 813, pp. 205-209, 2013.

[2] C. T.-C. Nguyen, MEMS technology for timing and frequency control, *IEEE transactions on ultrasonics, ferroelectrics, and frequency control,* Vol. 54, No. 2, pp. 251-270, 2007.

[3] S. Lucyszyn, Review of radio frequency microelectromechanical systems technology, *IEE Proceedings-Science, Measurement and Technology,* Vol. 151, No. 2, pp. 93-103, 2004.

[4] C. T. C. Nguyen, Transceiver front-end architectures using vibrating micromechanical signal processors, *RF Technologies for Low Power Wireless Communications*, pp. 411-461, 2001.

[5] J. M. Dewdney, Low loss VHF and UHF filters for wireless communications based on piezoelectrically-transduced micromechanical resonators, 2012.

[6] M. Xiao, A. Xu, Z. Sui, W. Zhang, H. Liu, C. Lee, Multifunctional MEMS, NEMS, micro/nano-structures enabled by piezoelectric and ferroelectric effects, *Nanoscale Horizons,* Vol. 10, No. 11, pp. 2744-2771, 2025.

[7] U. Rawat, *CMOS-MEMS for RF and Physical Sensing Applications*, Thesis, Purdue University, 2022.

[8] T. Zhang, J. Wu, J. Yang, G. Zhou, A MEMS comb drive resonator with electrically tunable nonlinearity, *Sensors and Actuators A: Physical*, pp. 117606, 2026.

[9] C. Tong, *Materials for high frequency filters*, in: *Advanced Materials and Components for 5G and Beyond*, Eds., pp. 109-141: Springer, 2022.

[10] J. Yang, *Integrated Ultra-High Q Bulk Acoustic Wave Resonators in Thick Monocrystalline Silicon Carbide*, Thesis, Georgia Institute of Technology, 2020.

[11] E. Aslan, E. Aslan, Engineering the boosting of the magnetic Purcell factor with a composite structure based on nanodisk and ring resonators, *Journal of Electromagnetic Waves and Applications,* Vol. 36, No. 10, pp. 1339-1351, 2022.

[12] M. Rana, R. Pande, K. Kukreti, Design of RF MEMS piezoelectric disk resonator for 5G communication, *Materials Today: Proceedings,* Vol. 73, pp. 13-17, 2023.

[13] T. Feng, Q. Yuan, D. Yu, B. Wu, H. Wang, Concepts and key technologies of microelectromechanical systems resonators, *Micromachines,* Vol. 13, No. 12, pp. 2195, 2022.

[14] S. T. Balghari, A. Ali, M. Gratuze, F. Nabki, Mechanical mode coupled piezo-on-silicon bulk acoustic wave MEMS resonators in tank configuration for Q-enhancement, *Journal of Microelectromechanical Systems*, 2025.

[15] Kurmendra, R. Kumar, Novel capacitance evaluation model for microelectromechanical switch considering fringe and effect of holes in pull-up and pull-down conditions, *Microsystem Technologies,* Vol. 26, No. 3, pp. 873-884, 2020.

[16] S. Saravanamurugan, J. Elango, M. Thenarasu, J. Petru, Reliability analysis of different geometric configurations of Helmholtz resonators for a sustainable performance, *Scientific Reports*, 2026.

[17] K. Kiani, A. Nikkhoo, On the limitations of linear beams for the problems of moving mass-beam interaction using a meshfree method, *Acta Mechanica Sinica,* Vol. 28, No. 1, pp. 164-179, 2012.

[18] S. N. Atluri, J. Cho, H.-G. Kim, Analysis of thin beams, using the meshless local Petrov–Galerkin method, with generalized moving least squares interpolations, *Computational mechanics,* Vol. 24, No. 5, pp. 334-347, 1999.

[19] K. Kiani, A nonlocal meshless solution for flexural vibrations of double-walled carbon nanotubes, *Applied Mathematics and Computation,* Vol. 234, pp. 557-578, 2014.

[20] K. Kiani, Free vibrations of elastically embedded stocky single-walled carbon nanotubes acted upon by a longitudinally varying magnetic field, *Meccanica,* Vol. 50, No. 12, pp. 3041-3067, 2015.

[21] J. Jam, Y. Kiani, Low velocity impact response of functionally graded carbon nanotube reinforced composite beams in thermal environment, *Composite Structures,* Vol. 132, pp. 35-43, 2015.

[22] K. Kiani, Thermo-elastic column buckling of tapered nanowires with axially varying material properties: a critical study on the roles of shear and surface energy, *Iranian Journal of Science and Technology, Transactions of Mechanical Engineering,* Vol. 43, No. 3, pp. 457-475, 2019.

[23] M. Bao, 2005, *Analysis and design principles of MEMS devices*, Elsevier,

[24] F. D. Bannon, J. R. Clark, C.-C. Nguyen, High-Q HF microelectromechanical filters, *IEEE Journal of solid-state circuits,* Vol. 35, No. 4, pp. 512-526, 2000.

[25] C. T.-C. Nguyen, Vibrating RF MEMS overview: applications to wireless communications, in *Proceeding of,* SPIE, pp. 11-25.

[26] C. T.-C. Nguyen, Micromachining technologies for miniaturized communication devices, in *Proceeding of,* SPIE, pp. 24-38.

[27] V. Harshey, A. Morankar, R. Patrikar, MEMS Resonator for RF Applications, in *Proceeding of.*

[28] S. D. Senturia, 2001, *Microsystem design*, Springer,

[29] G. M. Rebeiz, 2004, *RF MEMS: theory, design, and technology*, John Wiley & Sons,

[30] W.-L. Huang, Z. Ren, C. T.-C. Nguyen, Nickel vibrating micromechanical disk resonator with solid dielectric capacitive-transducer gap, in *Proceeding of,* IEEE, pp. 839-847.

[31] S. Chitsaz Charandabi, *Development of a Lorentz force drive system for a torsional paddle microresonator using Focused Ion Beam machining*, Thesis, University of Birmingham, 2014.

[32] V. Srikar, S. D. Senturia, Thermoelastic damping in fine-grained polysilicon flexural beam resonators, *Journal of microelectromechanical systems,* Vol. 11, No. 5, pp. 499-504, 2002.

[33] M. Bao, H. Yang, Squeeze film air damping in MEMS, *Sensors and Actuators A: Physical,* Vol. 136, No. 1, pp. 3-27, 2007.

[34] V. Cool, W. Jaspers, C. Claeys, E. Deckers, Topology optimization of locally resonant metamaterials for high modal effective mass, in *Proceeding of,* Elsevier*,* pp. 111192.

[35] M. Rahimi Dizadji, S. Wang, V. Jafarpour, D. A. Reynoso, H. Huang, Flexural Beams as Mechanical Fabry–Perot Resonators: A Theoretical Framework for Dispersive Waveguide-Based Sensing, *Sensors,* Vol. 26, No. 9, pp. 2622, 2026.

[36] R. Capuano, W. Lacarbonara, M. R. Hajj, On the use of effective mass in modeling undamped mass-in-mass metamaterials, *International Journal of Engineering Science,* Vol. 220, pp. 104447, 2026.

[37] L. Sang, M. Liao, X. Yang, H. Sun, J. Zhang, M. Sumiya, B. Shen, Strain-enhanced high Q-factor GaN micro-electromechanical resonator, *Science and Technology of Advanced Materials,* Vol. 21, No. 1, pp. 515-523, 2020.

[38] T. Kaisar, S. E. H. Yousuf, J. Lee, A. Qamar, M. Rais-Zadeh, S. Mandal, P. X.-L. Feng, Multiple stable oscillators referenced to the same multimode AlN/Si MEMS resonator with mode-dependent phase noise and frequency stability, in *Proceeding of,* IEEE*,* pp. 16.3. 1-16.3. 4.

[39] T. Mion, M. J. D'Agati, S. Sofronici, K. Bussmann, M. Staruch, J. L. Kost, K. Co, R. H. Olsson III, P. Finkel, High isolation, double-clamped, magnetoelectric microelectromechanical resonator magnetometer, *Sensors,* Vol. 23, No. 20, pp. 8626, 2023.

[40] T. Niu, N. Nagai, Y. Zhang, K. Hirakawa, Strong coherent energy exchange induced by the bending-bending mode-coupling effect in doubly clamped MEMS beam resonators, *Physical Review Applied,* Vol. 22, No. 6, pp. 064008, 2024.

[41] A. Garofalo, A. Muoio, S. Sapienza, M. Ferri, L. Belsito, A. Roncaglia, F. La Via, Model of Quality Factor for (111) 3C-SiC Double-Clamped Beams, *Micromachines,* Vol. 16, No. 2, pp. 148, 2025.

[42] J. Wang, Z. Ren, C.-C. Nguyen, 1.156-GHz self-aligned vibrating micromechanical disk resonator, *IEEE transactions on ultrasonics, ferroelectrics, and frequency control,* Vol. 51, No. 12, pp. 1607-1628, 2004.